Density functional study of structural trends for late-transition-metal 13-atom clusters

L.-L. Wang and D. D. Johnson
Department of Materials Science and Engineering, and the Frederick Seitz Materials Research Laboratory, University of Illinois, Urbana-Champaign, Illinois 61801, USA

(Received 9 February 2007; revised manuscript received 12 April 2007; published 6 June 2007)

Because reactivity increases as particle size decreases and competition between numerous structures are possible, which affects catalytic and magnetic properties, we study the structural trends of late-transition-metal 13-atom clusters using density functional theory within the generalized gradient approximation to exchange-correlation functional. We consider open structural motifs, such as bilayer and cubic (recently found to have lower energy), and find new bilayer candidates that are even lower in energy. To study the influence of *d*-orbital filling on structural trends, we focus on Pt, Pd, and Rh clusters and find several new, low-energy structures for Pt_{13} and Pd_{13} from searches using a first-principle molecular dynamics high-temperature annealing. We find that 13-atom clusters prefer less square-cubic order as the *d*-orbitals gradually fill in the order of Rh, Pt, and Pd, and generally, low symmetry, open structures are preferred to high symmetry, compact ones, a trend explained from their electronic structures. For completeness, we briefly comment on improved exchange-correlation functionals affects on cluster morphology.

DOI: 10.1103/PhysRevB.75.235405 PACS number(s): 61.46.Bc, 73.22.−f, 75.75.+a, 71.15.Mb

I. INTRODUCTION

Transition-metal (TM) nanoparticles have been intensively studied due to their important role in many fields of nanotechnology,[1] such as heterogeneous catalysis and magnetic storage. The properties of TM nanoparticles depend strongly on the interplay between geometric and electronic structures, and, hence, such studies have most interest in the properties of the lowest energy structure. The ground state (GS) structures of noble gas and simple electron metal clusters are often well described by either geometric or electronic-shell models. However, for TMs with significant contribution from localized *d* electrons, many studies[2–11] have shown that the GS structures are not determined by such models, and an universal model has yet to be found. Thus, searching for the GS structures of small TM clusters continues to attract a large amount of studies.

Experimental determination of GS structure for small TM clusters is difficult. Theory and first-principles calculations, such as density functional theory (DFT), are often used, which help to reveal the interplay between geometric and electronic structure. For example, many theoretical studies have found that for noble metal, such as Au, small clusters (less than 7 atoms) prefer planar structures due to the strong *s*-*d* hybridization.[12] Also, 13-atom TM clusters has been studied intensively because it is the first magic number according to geometric shell model to form high symmetric icosahedral (I_h) and cuboctahedral (O_h) structures. Recently, using DFT at the level of generalized gradient approximation (GGA), several groups have found that such compact and high-symmetry isomers are not the GS structures for late TMs. For noble metals, Oviedo *et al.*[2] have found that Cu_{13}, Ag_{13}, and Au_{13} prefer amorphous structures. For other late TMs, Chang and Chou[7] have found that an open, buckled bilayer structure [see Fig. 1 in Ref. 7] with lower symmetry is lower in energy than I_h structure. More surprisingly, for 4*d* and 5*d* late TMs with open *d* orbitals, such as, Ru, Rh, and Ir, Zhang *et al.*[3–5,13] and Bae *et al.*[8,9] have found that structures with maximum number of simple cubes are more stable than other structures, which we will denote as square-cubic order.

Such open bilayer and square-cubic structures for the TM clusters may not be too surprising considering that open *d* orbitals lead to directional bonding. The optimal interaction requires some, but not the maximum, number of nearest neighbors. Also, for *d* orbitals, the s-e_g and e_g-e_g hybridizations control the next-nearest neighbor interactions leading to fcc structure in a solid and similar structures in finite clusters. Bae *et al.*[9] have found that Rh_{13} cluster strongly prefers the square-cubic order, whereas, Zhang *et al.*[4] have found out that Pd clusters do not. So it appears that the structural habit of 13-atom cluster is largely influenced by the filling of *d* orbitals. Yet, the study by Zhang *et al.*[4] lacks a systematic search for the GS structures for 13-atom clusters, so no extensive comparison can be made.

Notably, all these studies, including the present one, use DFT within GGA. DFT-GGA has been shown to be very fruitful for bulk and surface calculations. But for small clusters, especially for small TM clusters with localized open *d* orbitals, normal GGA suffers from unphysical electron self-interactions (which decrease with increasing cluster size as the cluster approaches more "bulk" like hybridization when GGA is then more reliable for structural parameters and relative energetics). The electronic structures of small TM clusters with open *d* orbitals are multiconfigurational in nature. The strong electron-correlation effect must be treated carefully. In a recent study,[14] we have shown that the GS structures and properties of small nonmetallic Ru clusters depend sensitively on the exchange-correlation (XC) functional used in DFT. We have found that using the hybrid PBE0 functional[15] (which corrects partially the unphysical electron self-interaction) for Ru_2 and Ru_3 gives closer agreement to experiment and high-level quantum chemistry results, which treat strong electron correlation more rigorously than DFT. More importantly, we found that the PBE0 GS structure of Ru_4 changed from a square planar to a tetrahedron, due to the less s-e_g and e_g-e_g hybridization that causes bending along

the diagonal of the square. Our findings require that caution be used regarding the DFT studies that search for the GS structures of small TM clusters, in particular for systems approaching half-filling of the *d* bands, and that the structural trends found so far based on DFT-PW91 need to be examined further. However, GS searches for TM clusters more than a few atoms using high-level quantum chemistry methods or DFT hybrid functionals, like PBE0, B3LYP, or HSE,[16] are very expensive.

Thus, because DFT-PW91 is widely used, reported, and relied upon, it is worthwhile to find the structural trends at the level of DFT-PW91, especially comparing the different trends among different TMs due to *d*-orbital filling, which can be considered as a zeroth-order approximation for such trends. A comparative study of hybrid functionals (especially ones valid for metallic cases[17]) versus normal GGA for small clusters over the entire *d*-band series remains as future work.

In this paper, we use DFT-PW91 calculations to study the structural trends of 13-atom clusters for late TMs. We start with comparing two bilayer structures (see below) for group 7 to 11 elements and then, in more detail, we search for GS structures for Rh, Pt, and Pd, exhibiting increased filling of *d* orbitals (8, 9 to 10 electrons, respectively). We consider both newly found open bilayer structures and cubic structures with different symmetries as well as compact structures with high symmetry of I_h and O_h. In addition, we use first-principle molecular dynamics (MD) to do annealing-based searches for the GS structures. We found several new lowest-energy structures for Pt_{13} and Pd_{13} clusters. Structural trends are explained with analysis of both structural and electronic properties. Among these three late TMs, square-cubic order is more preferred for Rh with more empty *d* orbitals, while open amorphous structure is preferred for Pd with filled *d* orbitals. Pt is in between with some square-cubic order. We also analyze the structure-property correlations in details. The paper is organized beginning with a section on computational details, followed by the results, discussion and conclusions.

II. COMPUTATIONAL DETAILS

A. DFT calculations

We used DFT (Refs. 18 and 19) with PW91 exchange-correlation functional,[20] a plane-wave basis set and projector augmented wave method[21] as implemented in the Vienna Atomic Simulation Package (VASP)[22,23], where the core electrons are treated in the frozen-core approximation. We used a 300 eV (or more) kinetic energy cutoff, 20 Å cubic box with at least 12 Å of vacuum, and only sampled the gamma point in the Brillouin zone. Gaussian smearing of 0.05 eV is used for all calculations. Total energies were converged to 1 meV/atom with respect to size of vacuum and *k*-point mesh (Γ point was found sufficient), while magnitudes of force on each atom were reduced below 0.02 eV/Å via conjugate gradient. The total energy is referenced to the energy of the atom given by the pseudopotential generation. The magnetic moments are determined by relaxation from an initial default value set in the VASP code, not by fixed-moment calculations. The outermost *d* and *s* valence states were treated, and, for more accuracy, the semicore *p* states were included for Pd and Rh.

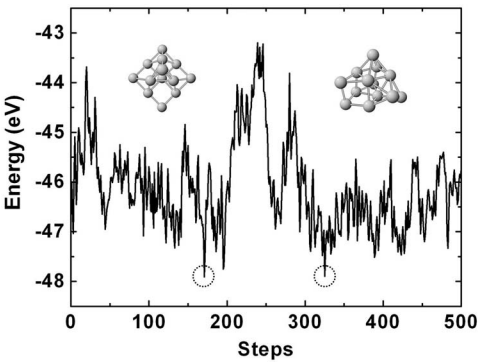

FIG. 1. First-principles MD of $Pt_{13}O_h$ cluster for 500 steps. Two low-energy instances are circled, with their corresponding structures after relaxation shown as insets.

For using first-principle MD to search for lowest-energy isomers, we started with a structure with high symmetry, such as O_h, and ran simulation at 2000 K for 4 to 10 picoseconds at time steps of 20 femtoseconds. Using this approach we can explore the potential-energy surface more efficiently and tabulate all visited low-energy structures to be studied more carefully later. As an example, in Fig. 1, we show a 500-step MD run for Pt_{13} cluster starting from the O_h structure. Then, we selected several structures having the lowest potential energies for further ionic relaxation. Two of such structures have been shown in the insets of Fig. 1. The search is stopped when no new, lower-energy structures appear in the finite simulation time span (typically 4 picoseconds).

B. Structure-property analysis

In the following analysis of the 13-atom isomers, we investigate total energy (in eV) relative to that of 13 single atoms, the isomer's magnetic moment in Bohr-magneton (μ_B/atom), along with a few meaningful structural parameters, i.e., average nearest-neighbor (NN) bond length (in Å), average NN coordination number, and mean interatomic distance (MIAD),[24] as well as the *s*-*d* hybridization index.[25,26] The MIAD of a cluster is defined as

$$\mathrm{MIAD} = N_{prs}^{-1} \sum_{n=1}^{N_{prs}} |\Delta R_n|, \tag{1}$$

where *n* runs over all pairs of atoms in the cluster and ΔR_n is the distance between each of those pairs. The MIAD then reflects the effective radius of a cluster, and permits, for example, an analysis of morphological change.[27] The lowering of the total energy by morphology change can be revealed to arise, for example, from decreasing of NN bond lengths, i.e., stronger atomic interactions. The *s*-*d* hybridization index for a 13-atom cluster, as defined by Häkkinen *et al.*,[25,26] is

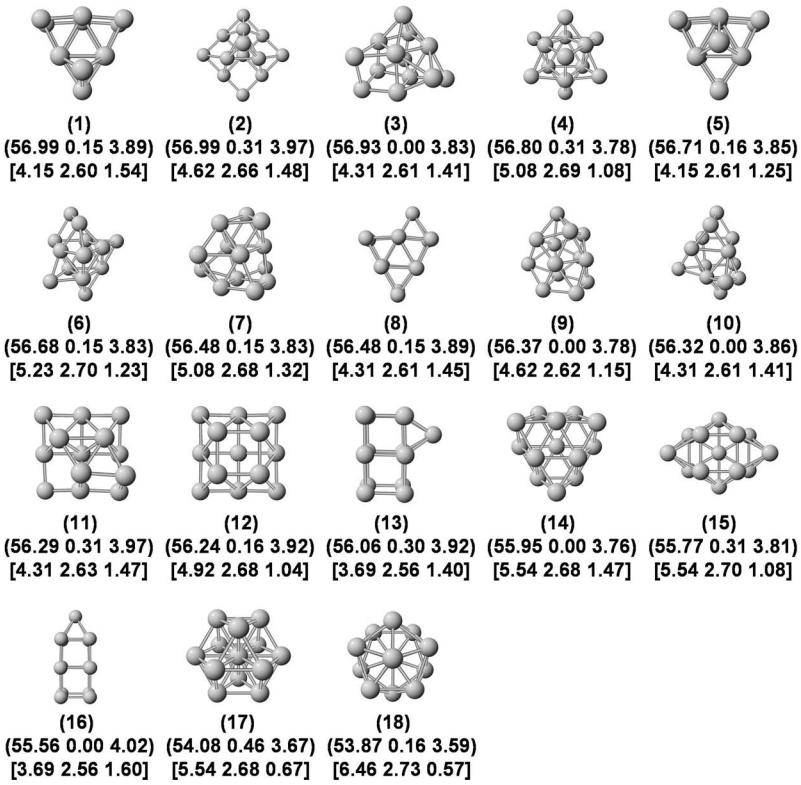

FIG. 2. Isomers of Pt_{13} cluster shown in the order of decreasing total energy. Properties listed below the structure are (in parentheses) energy (eV), magnetic moment (μ_B/atom), mean interatomic distance (Å), and [in brackets] first nearest-neighbor coordination number, first NN bond length (Å) and *s-d* hybridization index.

$$H_{sd} = \sum_{I=1}^{13} \sum_{i=1}^{\text{occ.}} w_{i,s}^{(I)} w_{i,d}^{(I)}, \tag{2}$$

where $w_{i,s}^{(I)}(w_{i,d}^{(I)})$ is the square of the projection of the ith Kohn-Sham orbital onto the s (d) spherical harmonic centered at the atom i, integrated over a sphere of radius equal to half of the shortest NN distance in each cluster. The H_{sd} was used by Chang and Chou[7] to indicate the increased stability of the alternative bilayer structures, in particular, a buckled bilayer cluster, compared to I_h cluster. However, the index cannot discern whether there are lower-energy bilayer structures that may happen to have similar structure parameter to a buckled bilayer one, for example, nor if there are lower-energy structures, as we show below. Nonetheless, the *s-d* hybridization index can be quite useful to indicate enhanced hybridization between various classes of isomers, which can correlate with stability.

III. RESULTS AND DISCUSSION

A. Overview of structural motifs

A review of the literature reveals at least three classes of structural motifs to consider when searching for the GS structure of late-TM 13-atom cluster. The first class is the compact high-symmetry O_h and I_h structures derived from the geometric shell model, in which 13-atoms is the smallest that these can occur. The second class is the open structures with maximum number of squares and cubes, i.e., square-cubic order, found to be very stable for Rh (the half-filled *d*-orbital case). The remaining structures comprise the third class, which are open structures having much lower symmetry than the first class, but that do not have as many square and cubes as is possible. The first two classes are easy to enumerate. However, the third class is the one with the most possible structures, including amorphous ones. To search in the third class, we employ two approaches. First, we find high-symmetry clusters by looking for all subgroups of O_h symmetry, which yields some new (intuitively) bilayer structures with lower energy. The other is a global search by first-principles MD using high-temperature annealing.

As an example, in Fig. 2, the structures and properties of the Pt_{13} clusters that we have found are listed in the order of decreasing stability. As mentioned earlier, to study the structural trend of the Pt_{13} cluster, we divide the 18 isomers into three classes. Isomers Fig. 2-(17) and (18) are compact structures with O_h and I_h symmetry, respectively. Isomers Fig. 2-(13) and (16) have open structures with a maximum number of simple cubes. In the remaining isomers of open structures, there are bilayer structures with symmetries of C_{2v} Fig. 2-(15), C_{3v} Fig. 2-(14) and C_{4v} Fig. 2-(12), which are subgroups of O_h. (In a private communication in 2005, we reported the C_{3v} structure to Chang and Chou for comparison to their C_{2v} structure for all the late TMs, and it has also been recently found via simulated annealing for Pt_{13}, Pd_{13} and Rh_{13} by Futschek, Marsman, and Hafner.[28,29]) From first-principle annealing, we also find many isomers with low-symmetry and open structures. We purposely single out the structures in the compact and cubic classes because their structures and properties are on the two extremes, having the largest and smallest first NN coordination number, respectively. The remaining structures are in between, some of which have a number of squares or cubes, i.e., a degree of square-cubic order.

TABLE I. Energy difference (ΔE) of C_{3v} bilayer structure and C_{2v} buckled bilayer structure versus element, along with the average NN bond lengths and magnetic moments per atom (in parenthesis). The trends within a group or period are evident, with C_{3v} lower than C_{2v} except for noble metals, where amorphous structure is then lowest (Ref. 2).

Group	Element	ΔE (eV)	C_{3v} Å (μ_B/atom)	C_{2v} Å (μ_B/atom)
7	Tc ($4d^5 5s^2$)	−1.88	2.54 (0.08)	2.55 (0.39)
	Re ($5d^5 6s^2$)	−2.08	2.57 (0.39)	2.57 (0.54)
8	Ru ($4d^7 5s^1$)	−0.94	2.53 (0.00)	2.52 (0.46)
	Os ($5d^6 6s^2$)	−1.32	2.54 (0.31)	2.55 (0.30)
9	Co ($3d^7 4s^2$)	−0.65	2.35 (2.08)	2.35 (1.92)
	Rh ($4d^8 5s^1$)	−0.21	2.62 (1.61)	2.61 (1.30)
	Ir ($5d^7 6s^2$)	−0.60	2.60 (0.85)	2.60 (0.85)
10	Pd ($4d^{10} 5s^0$)	−0.19	2.70 (0.46)	2.69 (0.31)
	Pt ($5d^9 6s^1$)	−0.18	2.68 (0.00)	2.70 (0.31)
11	Cu ($3d^{10} 4s^1$)	+0.05	2.46 (0.08)	2.46 (0.08)
	Ag ($4d^{10} 5s^1$)	+0.07	2.85 (0.08)	2.84 (0.08)
	Au ($5d^{10} 6s^1$)	+0.02	2.85 (0.08)	2.89 (0.08)

For bilayer structures, in general, one should consider (at the minimum) all the symmetry subgroups of O_h, which shows that the buckled bilayer C_{2v} structure found by Chang and Chou is not unique. In Table I, we list total-energy differences between C_{3v} Fig. 2-(14) and C_{2v} Fig. 2-(15) structures, their average first NN bond lengths and magnetic moments per atom, and compare these properties for the late TMs. Except for the noble metals, the C_{3v} is always preferred over C_{2v}. Similar to the C_{2v} structure, the C_{3v} structure is bilayer, with a 7-atom hexagonal and 6-atom triangular layers stacked cuboctahedrally, reminiscent of stacking of (111) closed-packed layers in bulk fcc or hcp. Numbers of first NN bonds in C_{3v} and C_{2v} structures are both 36. The hybridization index analysis used by Chang and Chou[7] still holds, of course, where C_{3v} and C_{2v} should have similar indexes as it reflects local bonding and structure (Chang has also confirmed this, private communication). Average bond lengths in C_{3v} and C_{2v} are very similar, but C_{3v} is a more natural structure to late TM, and the C_{3v} is preferred for TM with unfilled d levels. For metals with filled d's (Cu, Ag, and Au), the C_{2v} is barely preferred, but the GS is then really highly asymmetric or amorphous.[2]

As mentioned in the Introduction, because DFT-PW91 does not handle well the unphysical electronic self-interaction, especially for middle TM with half-filled d orbitals, we will focus on three late TMs of Pt, Pd and Rh for the remainder of the paper to find structural trend for 13-atom cluster.

B. Pt_{13} clusters

A Pt atom has the valence configuration of $5d^9 6s^1$. Among all the isomers shown in Fig. 2, the compact class has the highest energy, with O_h lower than I_h. Yet, the cubic class of clusters in Figs. 2-(13) and (16) with the maximum number of cubes has comparable energy with the open bilayer structures. Among the open bilayer structures, C_{4v} in Fig. 2-(12) has the lowest energy, followed by C_{3v} in Fig. 2-(14) and then C_{2v} in Fig. 2-(15). We note that the C_{2v}, i.e., the buckled bilayer structure suggested in Ref. 7, is not special. It actually has the highest energy among the bilayer structures, whose symmetries are subgroups of O_h.

More generally, via first-principle MD annealing, more unexpected motifs are identified, such as Figs. 2-(1) and (2), whose origin is not physically transparent and it does not have high symmetry. The isomers with low symmetry and open structures found by MD annealing have lower energy than all the isomers mentioned above. These structures have not been reported before, as far as we are aware. Among these open structures, the lowest-energy one is a bilayer of two 6-atom triangles stacked together in a mirrored configuration with one extra, capping atom on one of the corners (in a position of high electron density), see Fig. 2-(1), which we denoted as double triangle (DT) structure. This isomer is 2.91 eV lower than O_h. The DT structure is not surprising because our calculations and previous study[30] have shown that the 6-atom triangle is a very stable structure for Pt_6. On this stacked two 6-atom triangles, we put the extra Pt atom in three possible sites as seen in Figs. 2-(1), (5), and (8). We found isomer (1) has the lowest energy. The Pt–Pt bond lengths in the center of the cluster are significantly larger than the other bonds. Another isomer that is degenerate with DT has a bent 9-atom square with a 4-atom tetrahedron on top, see Fig. 2-(2). This isomer can be seen as derived from the bilayer C_{4v} structure in Fig. 1-(12). Both these and DT structures have some distorted squares, which shows that the square-cubic order does lower energy for Pt clusters.

Several properties of the Pt_{13} isomers are shown in Fig. 3 to correlate with energy. In Fig. 3(a), the structures and their magnetic moments are plotted versus energy. For low energy isomers, Pt_{13} tends to have the magnetic moment of roughly 0.2 μ_B per atom, where the lowest energy isomers approach a quenched moment, as in bulk Pt. In Fig. 3(b), the first NN bond length and coordination number are plotted versus the total energy. Similarly, the MIAD and the s-d hybridization index are compared in Fig. 3(c). Clearly, there is a good correlation in Fig. 3(b) between the first NN bond length and coordination number, as also shown directly in Fig. 3(d). The more open the structure, the shorter Pt–Pt bonds are to balance the fewer number of the first NN interactions. The compact and cubic classes are extreme examples with large coordination (large bond length) and small coordination (small bond length), respectively. The low energy structures are in between with medium first NN coordination number and bond length. There is some correlation between MIAD and the s-d hybridization index, especially between different classes of structure as shown in Fig. 3(c). The compact structures have much smaller s-d hybridization. Overall, there is little correlation between any of these properties with energy.

In Fig. 4, we plot the projected density of states (PDOS) on the atomic s, e_g and t_{2g} orbitals for three isomers in different structural classes, O_h in Fig. 2-(17), cubic in Fig. 2-(13) and DT in Fig. 2-(1). The e_g orbitals are d_{z^2} and $d_{x^2-y^2}$, and t_{2g} orbitals are d_{xy}, d_{xz} and d_{yz}. As shown in Fig. 4, among the three structures, cubic structure in Fig. 4(b) has the largest s-e_g hybridization, indicated by the largest DOS

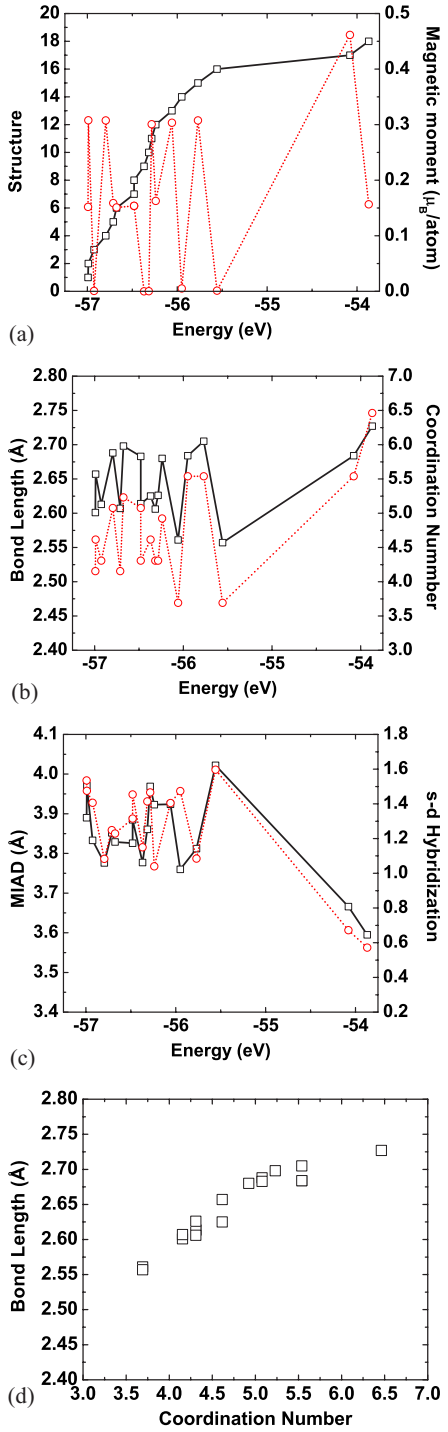

FIG. 3. (Color online) Structure-property correlation plots for Pt_{13} isomers. Isomers are numbered in the order of increasing energy, with corresponding structures shown in Fig. 2. In panel (a), (b), and (c), the x axis is the total energy of the isomer in negative value. For the left coordinates, the black solid line with squares in (a), (b), and (c) gives the number of the structure, the first nearest neighbor (NN) Pt-Pt bond length and the mean interatomic distance, respectively. For the right coordinates, the red dotted line with circles in (a), (b), and (c) gives the magnetic moment per atom, the first NN coordination number and the *s-d* hybridization index, respectively. (d) Correlation between the first NN bond length and coordination number.

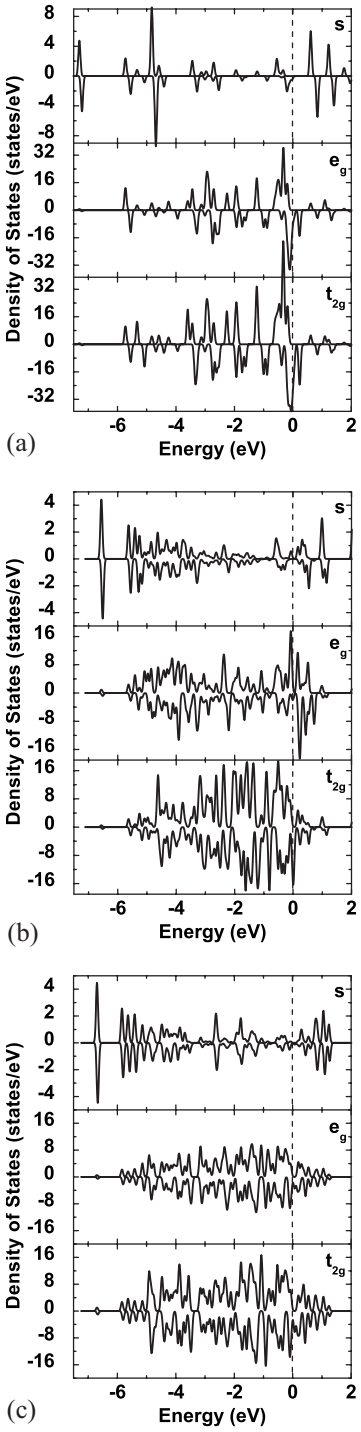

FIG. 4. Projected density of states (PDOS) on *s*, e_g and t_{2g} orbitals for Pt_{13} isomers, (a) O_h in Fig. 2-(17), (b) cubic in Fig. 2-(13), and (c) DT in Fig. 2-(1). The energy from lowest to highest is (c), (b), and (a).

overlap in the energy range from −6 to −3 eV. Since *s*-e_g hybridization favors the second NN interaction on an fcc lattice (see Fig. 3 of Ref. 14), it gives rise to square arrangements of atoms. Pt is a late TM with the anti-bonding *d* orbitals being filled. Large *s-d* hybridization helps to lower energy. As indicated in Fig. 3(c), open structures with large *s-d* hybridization index are generally lower in energy than

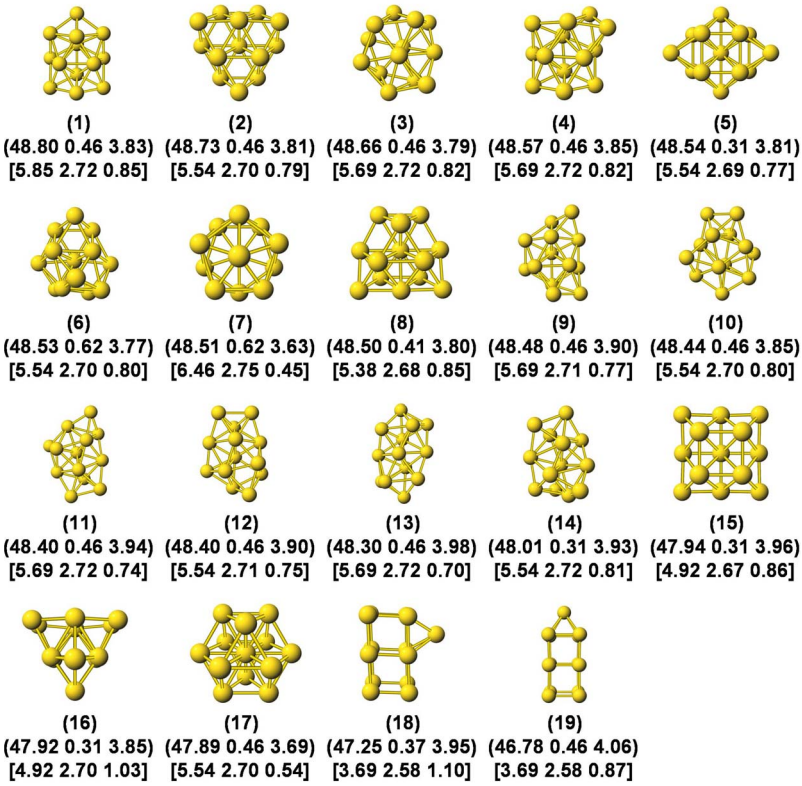

FIG. 5. (Color online) Isomers of Pd_{13} cluster shown in the order of decreasing total energy. The properties listed below the structure are the same as in Fig. 2.

the compact, high-symmetry isomers with small index. But the large *s-d* hybridization is at the cost of small *s-s* and *d-d* hybridization. The *s-d* hybridization cannot solely determine the lowest energy for Pt cluster. A compromise must be made among them. So DT structure in Fig. 2-(1) has the lowest energy, which has both a relatively large *s-d* hybridization index based on the squares in the structure and also relatively large *s-s* and *d-d* hybridization, as shown in Fig. 4(c) with the position of the low-lying *s* orbitals being lower than that in the cubic structure Fig. 4(b). Generally Pt_{13} does not prefer a cubic structure. The isomers only have some degree of square-cubic order.

C. Pd_{13} clusters

Compared with Pt in the same group, Pd has one more *d* and one less *s* electron in its valence configuration. The isomers of Pd_{13} and their properties are summarized in Figs. 5 and 6 in the order of increasing energy (decreased binding). Unlike Pt_{13}, the cubic structures in Figs. 5-(18) and (19) are the least stable for Pd_{13}. The cubic structure in Fig. 5-(18) also has the tendency to distort from the perfect cube toward a triangular structure. There are many low symmetry, open structures found by first-principles MD annealing that have no square or cubic component. This agrees with what Zhang *et al.*[4] found at the level of DFT-PW91—a Pd cluster does not prefer square-cubic order. Because Pd has filled *d* orbitals, Pd clusters favor amorphous structures as with noble metal clusters. For compact isomers, O_h has square-cubic components, while I_h does not, so I_h has much lower energy than O_h. This is why I_h has been long believed[31] to be the GS structure for Pd_{13}. Compared to Pt_{13}, the low-energy structures for Pd_{13} are ones with more closed-packing patterns. Among bilayer structures, C_{3v} in Fig. 5-(2) has the lowest energy, being just 0.07 eV above the lowest-energy structure shown in Fig. 5-(1).

The correlations among properties and energy are shown in Fig. 6. The low energy structures for Pd_{13} all tend to have the same magnetic moments of 0.46 μ_B/atom, which agrees well with the experimental data of 0.4 μ_B/atom.[32] Again there is a strong correlation between first NN bond length and coordination number as shown in both Figs. 6(b) and 6(d). There is a limited correlation between MIAD and *s-d* hybridization, but the extremes, such as cubic and compact classes, can be easily distinguished from the rest. Overall Pd_{13} tries to stay relatively compact and have a relatively large coordination number and large bond length. Although bulk fcc Pd has smaller lattice constant than bulk fcc Pt, it is interesting to note that Pd_{13} has a larger NN bond length on average than Pt_{13} with the same structure. This has to do with the more filling of the antibonding *d* orbitals of Pd than Pt in the clusters.

In Fig. 7, the PDOS of the selected structures in the three classes are shown. As seen in Fig. 7(b), for cubic structure the *s*-e_g hybridization (PDOS overlap) in low energy range is evident and also the bottom of the *s* levels are shifted to higher energy compared with the isomers without any square-cubic order, such as I_h in Fig. 7(a). Since cubic structures are the least stable among Pd_{13} isomers, the energy gain in *s*-e_g hybridization cannot compensate that is lost in *s-s* and *d-d* hybridizations. As shown by the PDOS in Fig. 7(c) for the lowest energy structure Fig. 5-(1) of Pd_{13}, unlike Pt, the dominant interaction in Pd clusters is the *s-s* and *d-d*, not the *s-d* hybridization. This is why the *s-d* hybridization index

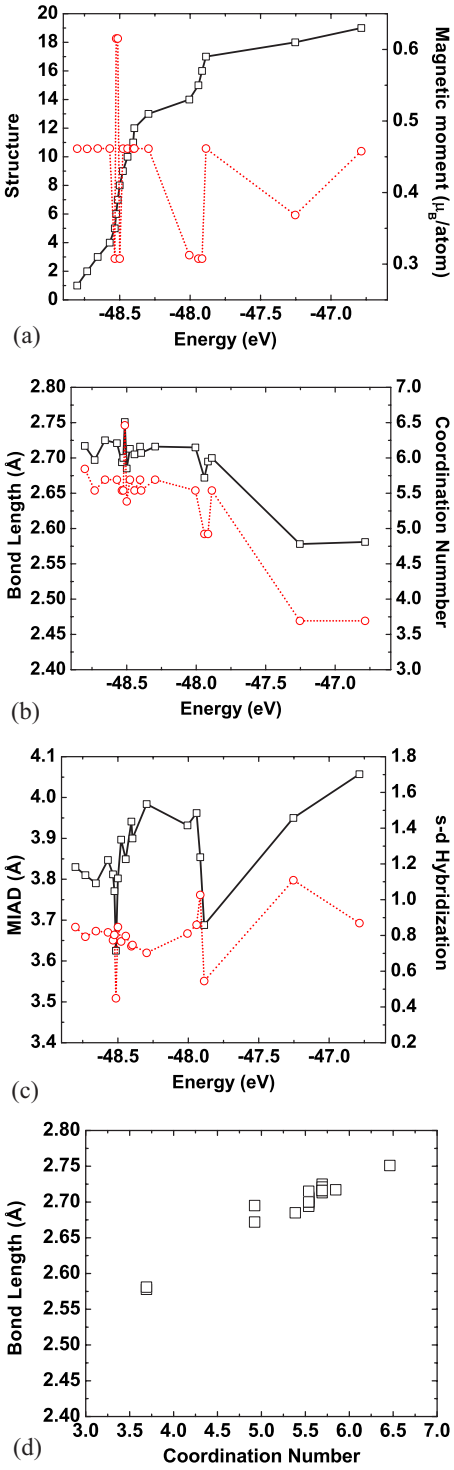

FIG. 6. (Color online) Structure-property correlation plots for Pd_{13} isomers. The isomers are numbered in the order of increasing energy, with corresponding structures shown in Fig. 5. In all panels, symbols and axis are the same as in Fig. 3.

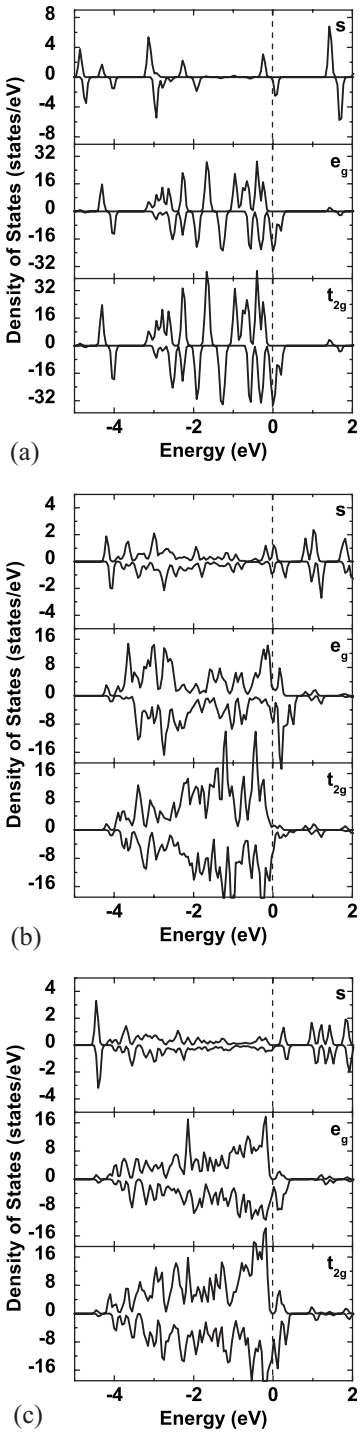

FIG. 7. PDOS on s, e_g and t_{2g} orbitals for Pd_{13} isomers, (a) I_h in Fig. 5-(7), (b) cubic in Fig. 5-(18), and (c) structure in Fig. 5-(1). The energy from lowest to highest is (c), (a), and (b).

does not correlate with energy order at all as shown in Fig. 6(c). For the same structure Pd_{13} has much smaller s-d hybridization than Pt_{13}. The structural habit of Pd is more close to noble metals than other TMs due to complete filling of the d orbitals.

D. Rh_{13} clusters

Moving to the other direction to reduce filling of d orbitals, we consider Rh_{13}, where Rh has one less d electron than Pt. Bae *et al.*[9] have found that Rh clusters prefer the square-cubic order at the level of DFT-PW91. As seen in Fig. 8, the open structures from (1) to (7), with some square-cubic com-

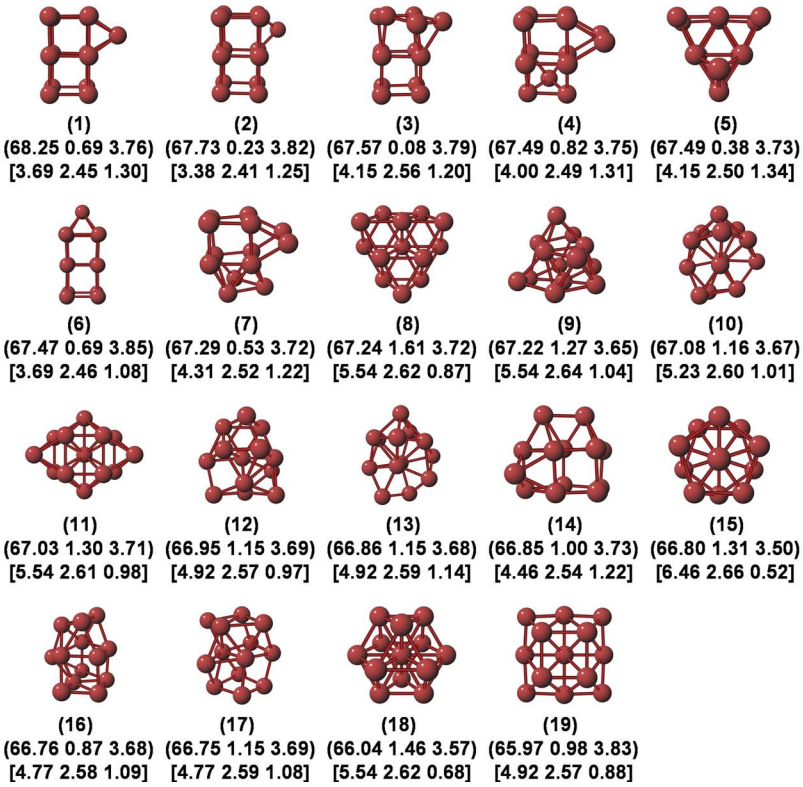

FIG. 8. (Color online) Isomers of Rh_{13} cluster shown in the order of decreasing total energy. The properties listed below the structure are the same as in Fig. 2.

ponents, indeed have lower energy than the others. The compact structures have higher energy than these open structures.

As shown in Fig. 9(a), the cubic structures with lower energy also have lower magnetic moments than the compact structures. Some cubic isomers even have lower magnetic moments than the experimental value of 0.48 μ_B/atom.[32] It is likely that what experiments measure is an ensemble average. As seen in Fig. 9(b), the open cubic structures have both smaller first NN coordination number and bond length. They correlate with each other well and also with the energy. Compared to Pt and Pd, Rh has a much stronger square-cubic order. The correlation between MIAD and *s*-*d* hybridization of Rh_{13} in Fig. 9(c) is similar to Pt_{13} and better than Pd_{13}.

The PDOS of the three selected structures are shown in Fig. 10. The strong *s*-e_g hybridization seen in Fig. 10(b) is the dominant factor over other hybridizations to give a much lower energy for structures with square-cubic order at the level of DFT-PW91. As shown in Fig. 10(c), for DT structure, with a less square-cubic order than the cubic structure, the *s*-e_g hybridization in low-energy range is less than that of the cubic structure in Fig. 10(b). For the three TMs studied here, in the order of the filling of *d* orbitals, Rh, Pt and Pd have less and less square-cubic order. As a confirmation, note that the DT structure is the lowest-energy structure for Pt_{13}, and the DT structure for Rh_{13} in Fig. 8-(5) has energy comparable with distorted cubic structures. But, in contrast, the Pd_{13} DT structure in Fig. 5-(16) has high energy, almost the same as the compact O_h structure Fig. 5-(17).

Thus, at the level of PW91 the trends and predictions from DFT are perfectly clear and understandable. While *s*-*d* hybridization index is useful, it does not always correlate with the lowest-energy structures, since stability and structure also depend upon *s*-*s* and *d*-*d* hybridization, as contrasted by Pd and Rh. For future work, it would be interesting to compare how these trends are affected by hybrid exchange-correlation functionals that alter the *s*-*d* hybridization in few-atom metallic clusters.[14]

IV. CONCLUSION

Using density functional theory calculations at the level of generalized gradient approximation (namely, PW91), we have studied the structural trends of late transition-metal Pt_{13}, Pd_{13} and Rh_{13} clusters, which represent the competing filling of *s* and *d* orbitals found more broadly for the entire late transition-metal series. For the entire late-TM series, we considered the open structural motifs, including the buckled bilayer structure, recently found to have lower energy by Chang and Chou.[7] For the bilayer structures, we considered other candidates with different symmetries from the previously studied one, especially those that are subgroups of the bulk O_h symmetry group, which, we stress, is a symmetry-based approach that should be used at a minimum when looking for lower-energy cluster morphologies. More generally, we utilized a more rapid, first-principle annealing approach to search for lower-energy structures, especially those that are typically not readily identified from simple hybridization arguments or intuition. We find that all the clusters prefer low symmetry, open structures rather than high symmetry, compact structures (as might be expected for almost filled *d*-band metals). For Pt_{13}, we found that both a stacked triangular structure and a square structure combined with a tetrahedron have the lowest energy. For Pd_{13}, we found that a

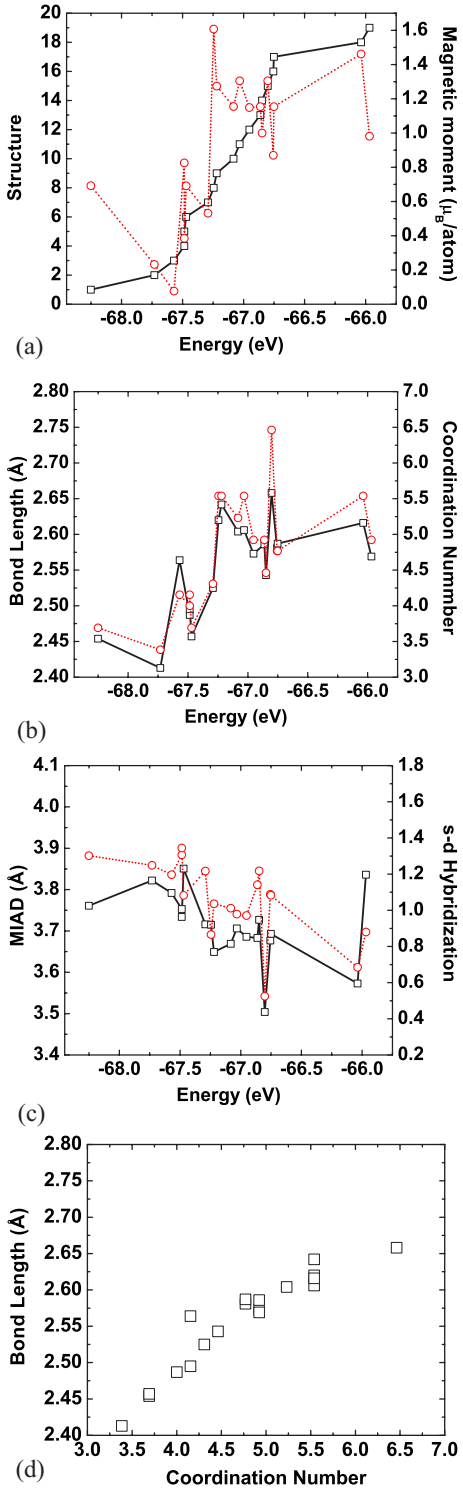

FIG. 9. (Color online) Plots of structure-property correlations of Rh_{13} isomers. The isomers are numbered in the order of increasing energy with corresponding structures shown in Fig. 8. In all panels, symbols and axis are the same as in Fig. 3.

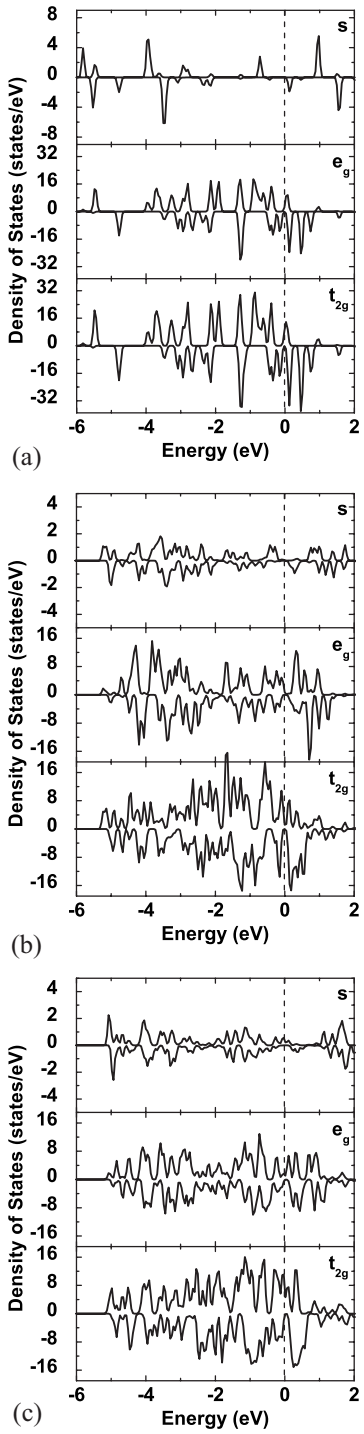

FIG. 10. PDOS on s, e_g and t_{2g} orbitals for Rh_{13} isomers, (a) I_h in Fig. 8-(15), (b) cubic in Fig. 8-(1) and (c) DT in Fig. 8-(5). The energy from lowest to highest is (b), (c), and (a).

low-symmetry structure with relatively closed packing has the lowest energy. For Rh_{13}, a cubic structure with a maximum number of simple cubes is found to be the lowest energy structure, in agreement with previous studies. More importantly, we studied the difference in the structural trends for the three metals within DFT-PW91. We found that, in the order of gradual filling of d orbitals, Rh, Pt, and Pd 13-atom clusters prefer less and less square-cubic order. This trend within DFT-PW91 is explained in the relative dominance of the s-d hybridization over the other contributions.

ACKNOWLEDGMENTS

This work was supported by the Department of Energy under Catalysis DE-FG02-03ER15476 and The Frederick Seitz Materials Research Laboratory at the University of Illinois under DEFG02-91ER45439. We also acknowledge computational support provided by the Materials Computation Center through NSF/ITR Grant No. DMR-0325939.

[1] F. Baletto and R. Ferrando, Rev. Mod. Phys. **77**, 371 (2005).
[2] J. Oviedo and R. E. Palmer, J. Chem. Phys. **117**, 9548 (2002).
[3] W. Q. Zhang, Q. F. Ge, and L. C. Wang, J. Chem. Phys. **118**, 5793 (2003).
[4] W. Q. Zhang, L. Xiao, Y. Hirata, T. Pawluk, and L. C. Wang, Chem. Phys. Lett. **383**, 67 (2004).
[5] L. Xiao and L. C. Wang, J. Phys. Chem. A **108**, 8605 (2004).
[6] E. Apra and A. Fortunelli, J. Phys. Chem. A **107**, 2934 (2003).
[7] C. M. Chang and M. Y. Chou, Phys. Rev. Lett. **93**, 133401 (2004).
[8] Y. C. Bae, H. Osanai, V. Kumar, and Y. Kawazoe, Phys. Rev. B **70**, 195413 (2004).
[9] Y. C. Bae, V. Kumar, H. Osanai, and Y. Kawazoe, Phys. Rev. B **72**, 125427 (2005).
[10] F. Aguilera-Granja, J. M. Montejano-Carrizalez, and R. A. Guirado-Lopez, Phys. Rev. B **73**, 115422 (2006).
[11] R. C. Longo and L. J. Gallego, Phys. Rev. B **74**, 193409 (2006).
[12] H. Hakkinen and U. Landman, Phys. Rev. B **62**, R2287 (2000).
[13] W. Q. Zhang, H. T. Zhao, and L. C. Wang, J. Phys. Chem. B **108**, 2140 (2004).
[14] L. L. Wang and D. D. Johnson, J. Phys. Chem. B **109**, 23113 (2005).
[15] C. Adamo and V. Barone, J. Chem. Phys. **110**, 6158 (1999).
[16] J. Heyd, G. E. Scuseria, and M. Ernzerhof, J. Chem. Phys. **118**, 8207 (2003).
[17] E. R. Batista, J. Heyd, R. G. Hennig, B. P. Uberuaga, R. L. Martin, G. E. Scuseria, C. J. Umrigar, and J. W. Wilkins, Phys. Rev. B **74**, 121102 (2006).
[18] P. Hohenberg and W. Kohn, Phys. Rev. B **136**, B864 (1964).
[19] W. Kohn and L. J. Sham, Phys. Rev. **140**, 1133 (1965).
[20] J. P. Perdew and Y. Wang, Phys. Rev. B **45**, 13244 (1992).
[21] P. E. Blöchl, Phys. Rev. B **50**, 17953 (1994).
[22] G. Kresse and J. Furthmüller, Comput. Mater. Sci. **6**, 15 (1996).
[23] G. Kresse and J. Furthmüller, Phys. Rev. B **54**, 11169 (1996).
[24] S. Kummel, J. Akola, and M. Manninen, Phys. Rev. Lett. **84**, 3827 (2000).
[25] H. Hakkinen, M. Moseler, and U. Landman, Phys. Rev. Lett. **89**, 033401 (2002).
[26] H. Hakkinen, B. Yoon, U. Landman, X. Li, H. J. Zhai, and L. S. Wang, J. Phys. Chem. A **107**, 6168 (2003).
[27] L. L. Wang and D. D. Johnson, J. Am. Chem. Soc. **129**, 3658 (2007).
[28] T. Futschek, M. Marsman, and J. Hafner, J. Phys.: Condens. Matter **17**, 5927 (2005).
[29] T. Futschek, J. Hafner, and M. Marsman, J. Phys.: Condens. Matter **18**, 9703 (2006).
[30] S. H. Yang, D. A. Drabold, J. B. Adams, P. Ordejon, and K. Glassford, J. Phys.: Condens. Matter **9**, L39 (1997).
[31] P. Nava, M. Sierka, and R. Ahlrichs, Phys. Chem. Chem. Phys. **5**, 3372 (2003).
[32] A. J. Cox, J. G. Louderback, S. E. Apsel, and L. A. Bloomfield, Phys. Rev. B **49**, 12295 (1994).